Log-Profile Analysis of the Near-Surface Layer and Air–Sea Turbulent Fluxes in Hurricanes Using Dropsondes

DANIEL E. WALLACE,[a,b] MARK A. BOURASSA,[a,b] HEATHER M. HOLBACH,[a,c,d] AMELIA BRYAN,[a,b] SINIL YANG,[e] AND BAEK-MIN KIM[f]

[a] *Center for Ocean-Atmospheric Prediction Studies, Florida State University, Tallahassee, Florida*
[b] *Department of Earth, Ocean and Atmospheric Science, Florida State University, Tallahassee, Florida*
[c] *Northern Gulf Institute, Tallahassee, Florida*
[d] *NOAA/OAR/Atlantic Oceanographic and Meteorological Laboratory, Miami, Florida*
[e] *APEC Climate Center, Busan, South Korea*
[f] *Division of Earth Environmental System Science Major of Environmental Atmospheric Sciences, Pukyong National University, Busan, South Korea*

(Manuscript received 4 January 2024, in final form 16 February 2026, accepted 29 May 2026)

ABSTRACT: Data collected from individual dropsondes within tropical cyclones are analyzed to better understand the near-surface profiles of wind speed, potential temperature, and humidity. The resulting fitting parameters are used to estimate surface fluxes of momentum, sensible heat, and latent heat within tropical cyclones. Vertical offsets of the profiles are calculated and described. Our methodology accounts for these offsets through a displacement height for each profile. Of 915 dropsonde profiles visually examined, 42.3% appeared to have log-like near-surface profiles. Good matches to theoretical profiles were found with only 95 (10.4%) profiles (25% of profiles that had data in the layer of interest). The boundary layer variables that we determine from an individual dropsonde are noisy because dropsondes do not capture a good sample of the mean boundary layer. Despite the weaknesses, means and medians constructed from the collection of processed dropsondes can be used to estimate values of boundary layer variables within tropical cyclones. Our analysis produces wind speed–dependent median boundary layer values within a range of uncertainty determined from the observations. Examples of the profiles, displacement heights, fluxes, drag coefficients, and the abovementioned problems are presented.

KEYWORDS: Atmosphere-ocean interaction; Hurricanes/typhoons; Aircraft observations; Dropsondes

1. Introduction

The boundary layer of tropical cyclones (TCs) is of great interest for many reasons: The wind speeds used to categorize the intensity of a storm are within this boundary layer (Saffir 1973; Simpson 1974), boundary layer turbulent fluxes can be used to estimate the maximum potential intensity (Emanuel 1988) and might be related to intensity change (Emanuel 1986, 1995; Shen and Ginis 2003), the variability of these fluxes around the storm is controversial (Powell 2006; Holthuijsen et al. 2012), and spray generated by extreme winds could modify the boundary layer (Andreas 1992; Andreas et al. 1995; Andreas and Emanuel 2001) and storm intensity (Yang et al. 2024, 2025). Our knowledge of this boundary layer is relatively poor because the weather conditions are extremely challenging for in situ and satellite observations (Bourassa et al. 2019 and references therein). Ships tend to avoid severe weather, and in recent years, forecasts have provided sufficient warning to do so. Hurricane winds are observed by buoys when a storm center passes nearby, but buoy measurements are often suspect due to tilting of the buoy and uncertainties in its measurement height in high waves (Wright et al. 2021). When exposed to extreme winds (and the resulting currents), excess tension on the anchor chain pulls the buoy down at an angle. For instance, when Hurricane Katrina (2005) passed over observational buoys, sustained tilts of 15°–18° occurred (Howden et al. 2008; Bender et al. 2010). Satellite data for extreme winds are usually calibrated with measurements from reconnaissance aircraft, including vertical profiles measured by launching a disposable device with an array of sensors called a GPS Dropwindsonde (also called dropsonde and sonde) (Hock and Franklin 1999). The boundary layer profiles of pressure, wind speed, temperature, and humidity from individual dropsondes are used to demonstrate a methodology (a proof of concept), constrained by Monin–Obukhov similarity theory (MOST), for extracting TC boundary layer characteristics. A more rigorous study would use all available dropsondes and automatically identify log layers rather than manually identifying these layers as done in this study. The results of this study indicate that developing a tool to identify such layers would be beneficial.

The National Hurricane Center (NHC) uses an official definition of a peak 1-min-average wind speed as observed at the standard meteorological height of 10 m (NOAA-NHC 2021). This wind speed is important for categorizing the intensity and structure of a storm and for emergency planning. Dropsonde-based surface wind data are also used to calibrate (or validate) remotely sensed winds. One of the remote sensing tools for measuring surface wind speeds from aircraft, designed specifically for TC conditions, is the Stepped-Frequency Microwave

Denotes content that is immediately available upon publication as open access.

Corresponding author: Daniel Wallace, dwallace@coaps.fsu.edu

DOI: 10.1175/JTECH-D-24-0002.1

Radiometer (SFMR) (Uhlhorn and Black 2003). This device passively measures the brightness temperature of the surface, which is responsive to the fraction of whitewater coverage, an indicator of surface wind speed. Converting from measured radiation to wind speed requires good calibration and a complex algorithm that has been trained with dropsonde data (Uhlhorn and Black 2003; Uhlhorn et al. 2007; Klotz and Uhlhorn 2014). Extreme winds measured by satellite are often calibrated to SFMR winds and hence traced back to dropsonde winds.

The level of the surface (and subsequent heights above) measured by a dropsonde is subject to an unavoidable uncertainty (i.e., random error) of roughly 5 m (V. Holger 2021, personal communication) for moderate wind conditions. The same source has also expressed concerns about systematic errors for extreme wind conditions and concern that for these conditions, our displacement heights (a vertical offset of the log profile) could be interpreted as a combination of random and substantial positive systematic errors in the dropsonde heights (discussed more in sections 4b and 5a). Such errors would make it difficult to interpret mean vertical offsets in the context of processes. Our analysis technique is designed to account for these offsets relative to a mean ocean surface.

Natural variability, presumably associated with rolls and turbulence, can cause considerable variability within the heights that we are examining. This variability and the vertical offset mentioned above combine to make it impractical to treat the wind speeds near the dropsonde's height of 10 m as an estimate of mean wind speed at a height of 10 m. Consequently, layer averages have been commonly used to estimate 10-m mean winds from dropsonde data (Franklin et al. 2003). Two such approaches are currently in use operationally. The first, considered more conservative, averages the lowest 500 m, the approximate depth of the mean boundary layer (MBL). The second, the WL150, considers the lowest measured 150 m (Franklin et al. 2003). Both approaches use a reduction coefficient (Uhlhorn et al. 2007; Franklin et al. 2003), associated with the mean height of the observations, to estimate surface (10 m) values from the mean layer average.

Figure 1 shows an example of the lower portion of a wind speed profile in a TC. The lowest 150-m layer (below the dashed line) encompasses either multiple easily identifiable dynamical regimes or eddy-related perturbations from MOST. The profile in the WL150 calculation need not be consistent with MOST. We will discuss consistency between our estimates of 10-m winds and the WL150 winds used to calibrate the SFMR in section 5c.

It has often been suggested that layers of sea spray can have a large impact on the near-surface wind speed profile (Andreas 1992; Fairall et al. 1994; Andreas et al. 1995; Andreas and Emanuel 2001). The impact of spray on a wind profile including the logarithmic layer (hereafter log layer) remains an open question. Presumably, characteristics of the log profile (described in section 4b) would change due to spray. Investigation of spray impacts on a wind profile from a dropsonde are further complicated by concerns about the recorded wind speed, errors in height above the surface (discussed in section 5a), and the inability to identify the amount of spray. The values of the drag coefficient

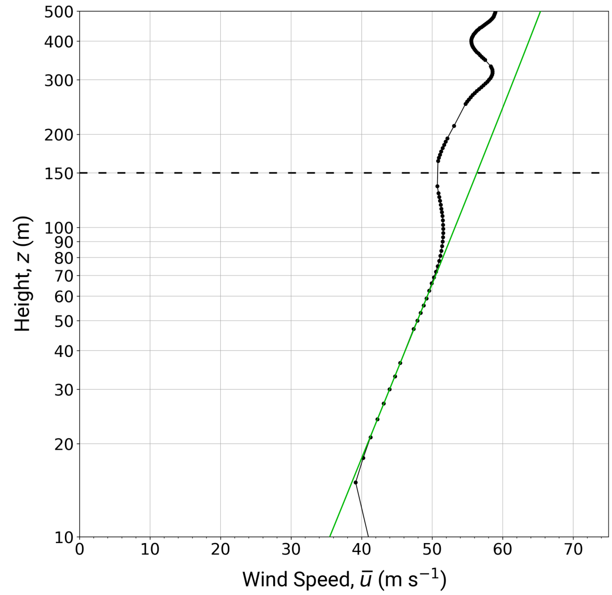

FIG. 1. Vertical profile from dropsonde D20201009_112638 dropped by reconnaissance aircraft NOAA42 into Hurricane Delta on 9 Oct 2020. The MBL calculations use all observations below 500 m. The lowest 150 m of observations are used in WL150 calculations (below the dashed line). The wind profile calculated from our method (green line; see section 4b for details) extrapolated to 10 m is 35.5 m s^{-1}. For comparison, the layer averages are MBL_{10} = 42.4 m s^{-1} and $\mathrm{WL150}_{10}$ = 41.0 m s^{-1}.

(section 5d), turbulent heat fluxes (section 5e), and displacement height (section 5a), examined as a function of wind speeds, are likely to contain the largest signal of modification due to spray, although dropsonde data alone cannot be used to directly test a dependence on spray.

There are several innovations in our approach (section 4). Our methodology is to solve for profiles, constrained to be consistent with MOST, that are best fits to dropsonde data. One innovation is that we consider displacement height: The World Meteorological Organization (WMO) defines surface winds with respect to their height within the log layer, where the presumed governing physics is applicable. Specifically, the WMO defines surface winds as 10 m above the displacement height (Harper et al. 2010), which is defined as the height at which the log layer extrapolates to a surface speed. This displacement height could help account for hypothetical wave or spray-induced vertical displacement of the wind profiles. It can also account for errors in identification of the surface in dropsonde data. A dropsonde's "surface" is defined as the height where it strikes water. Striking wave crests and troughs would displace the apparent surface too high or too low, respectively. Our calculated displacement heights (section 5a) are likely influenced by this definition. Our methodology can also adjust for other errors in surface height associated with hypothetical spray layers or problems and processes yet to be identified. Another innovation is that our MOST-based solution accounts for boundary layer stratification, whereas prior approaches assume a neutral profile (sections 4b and 5b).

One benefit of our MOST-based analysis is a 10-m wind that we argue improves upon the observed wind at the height a dropsonde indicates is 10 m. Earlier analyses of dropsonde data (WL500; Franklin et al. 2003) found using the sonde winds at 10 m to be less desirable than a modified average over 500 m or 150 m. Our analysis (section 5c) strongly supports Franklin et al.'s conclusion, provides an alternative estimate of this wind speed, points to small, but systematic differences from the WL150 for wind speeds > 35 m s^{-1}, and points to greater systematic errors for wind speeds $>$ 50 m s^{-1}. Second, by considering individual profiles instead of aggregate mean profiles as has been done previously (i.e., Powell et al. 2003; Holthuijsen et al. 2012; Richter et al. 2021) with log-profile analyses, we will be able to individually analyze dynamical features such as biases in dropsonde heights. Third, our methodology does not prescribe neutral stratification and can be used to estimate stratification. Similar to prior log-layer methodologies, surface turbulent fluxes and related transfer coefficients can be determined from the output of solutions for log profiles of wind speed, temperature, and moisture. Ideally, further application of this method will facilitate a better understanding of how energy is transferred at the surface interface within these storms. Our drag coefficients (section 5d) for wind speeds from 10 to 20 m s^{-1} are remarkably similar to well-accepted in situ observations (e.g., Large and Pond 1981; Smith 1988). We confirm the weak importance of performing analyses that consider boundary layer stratification (section 5b) and find that proper assignment of the surface height (section 5a) likely has greater impact on these analyses.

2. Theory for near-surface boundary layers

a. Monin–Obukhov similarity theory

MOST relates the mean vertical profiles of wind speed, potential temperature, specific humidity, and surface turbulent fluxes to roughness length and boundary layer stratification (Monin and Obukhov 1954; Foken 2006). Mean flows in the log layer agree with MOST in numerous field experiments (e.g., Businger et al. 1971; Kaimal et al. 1976). MOST requires horizontal homogeneity of the properties being considered. Variability within ensembles of profiles is due to eddies with time scales of variability that grow with increasing distance from the surface (Stull 1988a). An outcome of MOST is that in the lower portion of the boundary layer, the mean values of wind speed, potential temperature, and specific humidity are logarithmic functions of height, while vertical fluxes (e.g., stress, sensible heat, and latent heat) are independent of height within this log layer. This theory applies to heights above where winds have to flow around surface features, up to heights where Ekman processes dominate motion (Stull 1988b).

b. MOST parameterizations of log profiles

There are log-profile equations in MOST related to mean wind speed [Eq. (1)], potential temperature [Eq. (2)], and specific humidity [Eq. (3)]. The equations presented here are adapted from previous work studying log-profile parameters (Covey 1983; Bourassa 2000), which were based on early work on this topic (Prandtl 1925; Covey 1983; Stull 1988b). Values at the height to which the log layer is extrapolated downward (typically extrapolated to the mean surface value) are boundary conditions (limits of integration) in these solutions. While these values are normally included for profiles of potential temperature and humidity, they are usually not included for wind speed because the speed of the surface is zero over land and small over the ocean. Surface currents were included in the flux equations of Liu et al. (1979) and first shown to be important in observations by Chou (1993). Bourassa et al. (1999) described current-relative winds as important for making these equations independent of the Newtonian frame of reference and for determining roughness length. The vertically integrated impact of atmospheric dynamic stratification adjustment (Ψ) is also added using Liu's adaptation of L [Eq. (4)]. Finally, any vertical displacement of the profile, d, is considered. An idealized example is shown in Fig. 2:

$$\overline{u}_i = \overline{u}_d + \frac{u_*}{k}\left[\ln\left(\frac{z_i - d}{z_0} + 1\right) - \Psi_M(L, z_i, d)\right], \qquad (1)$$

$$\overline{\theta}_i = \overline{\theta}_d + \frac{\theta_*}{k}\left[\ln\left(\frac{z_i - d}{z_{0_\theta}} + 1\right) - \Psi_H(L, z_i, d)\right], \qquad (2)$$

$$\overline{q}_i = \overline{q}_d + \frac{q_*}{k}\left[\ln\left(\frac{z_i - d}{z_{0_q}} + 1\right) - \Psi_E(L, z_i, d)\right], \qquad (3)$$

$$L = \frac{\overline{\theta}_d(1 + 0.61\overline{q}_d)u_*^2}{k_v g[\theta_*(1 - 0.61q_*) + 0.61\overline{\theta}_d q_*]}. \qquad (4)$$

The subscript i indicates different heights (z_i). The subscript d indicates the value of the variable extrapolated down to the displacement height (d), which over water is normally treated as the value at the water surface. Dimensional scaling parameters (u_*, θ_*, q_*) and roughness lengths (z_o, z_{o_θ}, z_{o_q}) combine to describe the shape of the neutral profiles. Variables are explained in the appendix. The + 1 in the log terms are normally dropped because it is tiny compared to first term in the natural log. We retain the + 1 to ensure the solutions do not involve a log of negative number.

c. Stratification parameterizations

Monin and Obukhov argued that within the log layer, the dependence of stratification on the vertical gradients of wind speed and potential temperature could be described with a dimensionless parameter (z/L) derived from the height and the length scale (L) defined in their earlier work (Obukhov 1946, 1971). The log-profile equations of wind speed, potential temperature, and specific humidity [Eqs. (1)–(3)] all contain a stratification term (Ψ). This term is a function of height (z), the Obukhov length (L), and the roughness length (z_0) in the form of z/L and z_0/L. The latter is usually dropped because it is negligible over the ocean—even in TCs. Hence, stratification adjustments become functions of only z and L, where L is a function of fitting parameters from all three profiles [Eq. (4)]. This means that the profiles are all intrinsically

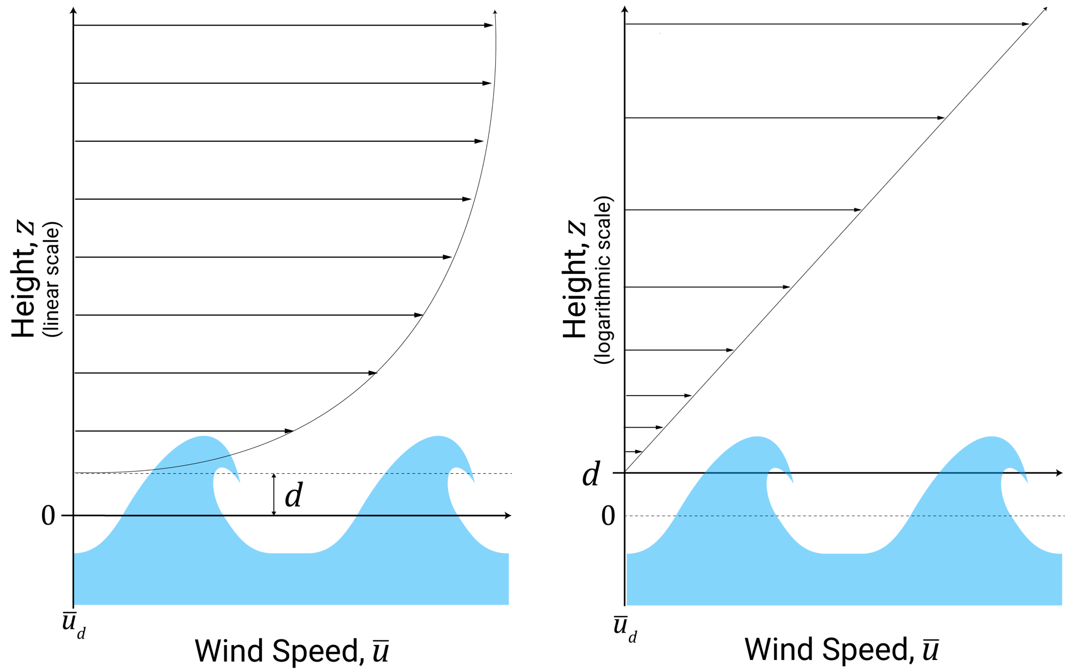

FIG. 2. Idealized log profile of wind, with speed $\overline{u}$ and height z. The surface ($z = 0$) represents calm sea level. The wind waves pictured displace the profile upward to a fraction of the significant wave height as previously suggested (Bourassa 2006). Displacement height d is the height where the log profile extrapolates to a speed of zero relative to the surface. (left) A linear scale with height relative to the surface; (right) a logarithmic scale with the height relative to d.

linked together and must be solved simultaneously if nonneutral conditions are assumed (i.e., $\Psi \neq 0$).

To model the dependence of Ψ on z/L, we use stratification parameterizations in the Coupled Ocean–Atmosphere Response Experiment (COARE) 3.0 flux algorithm (Fairall et al. 2003). For unstable conditions $L < 0$, the following adaptations are used (Grachev et al. 2000), modified with the approximation that $z_0/L = 0$:

$$\Psi_M = -2\ln\left(\frac{\zeta_M}{2}\right) - \ln\left(\frac{\zeta_M^2}{2}\right) + 2\tan^{-1}(\zeta_M), \tag{5}$$

where

$$\zeta_M = \left[1 - 16\left(\frac{z-d}{L}\right)\right]^{1/4}, \tag{6}$$

$$\Psi_{H,E} = -2\ln\left(\frac{\zeta_{H,E}}{2}\right), \tag{7}$$

where

$$\zeta_{H,E} = \left[1 - 16\left(\frac{z-d}{L}\right)\right]^{1/2}. \tag{8}$$

For stable conditions ($L > 0$), we use the following parameterizations (Beljaars and Holtslag 1991):

$$\Psi_M = -\frac{z-d}{L} - 0.667\left(\frac{z-d}{L} - 14.29\right)\exp\left(-\frac{z-d}{L}\right) - 9.53, \tag{9}$$

$$\Psi_{H,E} = -\left(1 + \frac{2}{3}\frac{z-d}{L}\right)^{3/2} - 0.667\left(\frac{z-d}{L} - 14.29\right)\exp\left(-\frac{z-d}{L}\right) - 8.53. \tag{10}$$

One novel aspect of these stratification equations is that we have made z relative to the displacement height, rather than ignoring d. This is an important distinction if the displacement height is substantially nonzero.

d. Turbulent fluxes

Surface turbulent fluxes of momentum [Eq. (11)], sensible heat [Eq. (12)], and latent heat [Eq. (13)] are calculated from the dimensional scaling parameters (u_*, θ_*, and q_*):

$$\tau = \rho|u_*|u_*, \tag{11}$$

$$Q_{\text{sen}} = -\rho C_P|u_*|\theta_*, \tag{12}$$

$$Q_{\text{lat}} = -\rho L_V|u_*|q_*. \tag{13}$$

These formulas also require the air density ρ, calculated using the ideal gas law and temperature and pressure measurements

TABLE 1. Intensity statistics for all 387 dropsondes that were successfully processed (full set) and the 95 dropsondes that remained after QC (QC set). Storm intensity categories, based on peak 1-min 10-m winds from the NOAA best-track database (Knapp et al. 2010), are defined using the Saffir–Simpson hurricane wind scale (Saffir 1973; Simpson 1974; Schott et al. 2019).

Intensity	Full set	QC set	Intensity	Full set	QC set
Tropical storm	11	1	Category 3 hurricane	96	21
Category 1 hurricane	34	5	Category 4 hurricane	154	41
Category 2 hurricane	63	17	Category 5 hurricane	29	10

from the dropsonde. Two near constants are also used, the specific heat capacity of dry air, $C_P = 1005.7\ \mathrm{J\ kg^{-1}\ K^{-1}}$, and the latent heat of vaporization of water, $L_V = 2.501 \times 10^6\ \mathrm{J\ kg^{-1}}$.

e. Transfer coefficients

We can also determine the value of wind, potential temperature, and humidity at any height within the log layer. For example, a wind speed at 10-m height (relative to the displacement height) is often used in atmospheric models and for forcing ocean models. It is also used to calculate the transfer coefficients (described below) which are used to estimate turbulent fluxes in a computationally efficient manner. These winds, potential temperatures, and humidities can be calculated by using Eqs. (1)–(3), respectively, at a height of $z - d = 10$ m.

The coefficient of drag C_D is a key parameter in most TC models and has been estimated from observations and modeled in many studies for decades. The C_D is calculated from friction velocity and the vertical wind shear:

$$C_D(z - d = 10\,\mathrm{m}) = \left(\frac{u_*}{\overline{u}_{10} - \overline{u}_d}\right)^2. \tag{14}$$

Similarly, the heat and moisture transfer coefficients (C_H and C_E) are

$$C_H(z - d = 10\,\mathrm{m}) = \left|\frac{u_*}{\overline{u}_{10} - \overline{u}_d}\right|\left(\frac{\theta_*}{\overline{\theta}_{10} - \overline{\theta}_d}\right), \tag{15}$$

$$C_E(z - d = 10\,\mathrm{m}) = \left|\frac{u_*}{\overline{u}_{10} - \overline{u}_d}\right|\left(\frac{q_*}{\overline{q}_{10} - \overline{q}_d}\right). \tag{16}$$

3. Dropsonde data

This study uses dropsondes launched directly into TCs by NOAA Lockheed WP-3D Orion aircraft (NOAA42 and NOAA43). Dropsondes are selected from flights from 2018 to 2022, and there are a few extreme cases from 2004 to 2017. The RD93 sonde was used from the late 1990s until 2010, RD94 from 2010 to 2019, and RD41 from 2019 to 2024. Future work should expand the scope of the data sources to include dropsondes processed by the U.S. Air Force Reserve 53rd Weather Reconnaissance Squadron.

Dropsondes collect observations of the vertical structure of the atmosphere. Position and wind data are sampled four times per second (4 Hz) and temperature, moisture, and pressure two times per second (2 Hz) since 2010 (Hock and Franklin 1999; Wang et al. 2015; UCAR/NCAR–Earth Observing Laboratory 1993). Prior to 2010, the wind data were sampled at a rate of 2 Hz. The raw data transmitted by the dropsondes to the aircraft are then processed through a program called the Atmospheric Sounding Processing Environment (ASPEN). ASPEN attempts to detect where the dropsonde hits the surface and flags anything beyond that for removal—dropsondes can float and continue transmitting for a while before sinking and losing signal. Our estimates of displacement height will include errors in the assessment of the height relative to the mean surface, greatly reducing the impact of these errors on surface relative wind speeds, transfer coefficients, and fluxes. ASPEN will also flag all data points that are irregular. This can mean either a suspect measurement that changes too drastically between observed heights to be physically plausible or that the GPS receiver was not connected to enough satellites to confidently acquire position (Martin and Suhr 2021). All automatic checks are reviewed and confirmed by the processing scientist.

Another advantage of ASPEN is a correction of the vertical position to account for a delay between recording data and recording the vertical position. ASPEN also applies smoothing to the raw dropsonde data, which can potentially remove or blur features from the raw data. Of particular importance to this research, vertical profiles of wind speed ($\overline{u}$), potential temperature ($\overline{\theta}$), and specific humidity ($\overline{q}$) are provided or can be calculated from available data. The latter two variables are not directly measured by the dropsondes, but are calculated in this study from dropsonde observations. Potential temperature is calculated from the pressure, surface temperature, and a reference pressure (10^5 Pa). Specific humidity is determined from the vapor pressure, using Buck's (1981) approximation of the Clausius–Clapeyron equation, the dropsonde observations of pressure, air temperature, and relative humidity.

In this study, a total of 915 dropsonde data files are plotted and reviewed. Of these, 387, or about 42.3%, are processed using the methodology outlined. Only 10.4% of the original total (24.5% of the processed sondes) pass our quality control (QC) checks (section 4d). Dropsonde profiles that contain an approximately log-linear layer of at least four data points in each of the three vertical profiles of wind, potential temperature, and specific humidity are input into the calculation program as described in section 4b. The successfully processed profiles are sorted by peak storm intensity during the flight (Table 1) and the launch location within the storm (Table 2). The percentages of various categories do not represent the climatology of TCs in general. Higher category storms are preferentially selected in this study because of the operational targeting of dropsondes and because we gave higher wind speeds a priority to improve our statistics for those conditions.

TABLE 2. Storm-relative radial (left) and azimuthal (right) position for all 387 dropsondes that were successfully processed (full set) and the 95 dropsondes that remained after QC (QC set). Azimuthal storm sector definitions adapted from Black et al. (2007) using storm-motion-relative headings of 20°–150° for the right sector, 150°–240° for the rear sector, and 240°–20° for the left-front sector.

Radial sector	Full set	QC set	Azimuthal sector	Full set	QC set
Outer bands	197	33	Left front	151	36
Eyewall	151	53	Right	157	42
Eye/other	39	9	Rear	79	17

A more complete dataset (Ahern et al. 2019) shows less of a bias toward higher categories.

Of the dropsondes considered for inclusion in our study, total sensor failure for one of the variables accounted for 10.4% of the unused data. Partial sensor failure (at the heights of interest) accounts for 27.3% of the culled profiles (i.e., 37.7% were unusable because of missing data). The remainder of the culled data (62.3% of the culled data, 35.8% of the dropsondes examined) was unprocessed because of the shape of the profile. Some examples of unsuitable profiles are cases where the wind speed decreased with increased height throughout the layer of interest. In others there were layers that looked log-like, but with too few observations to be useful (23.8% of the profiles). In other words, a log-like layer could not be identified over a sufficiently thick layer. All dropsonde profiles examined with loosely log-like shapes for each of the three variables (42.3% of sondes without missing data) were included in this analysis. This percentage compares favorably with the dropsonde composite dataset compiled in Ahern et al. (2019). They used approximately 25.7% of the 12 045 dropsondes to create their composite dataset.

Problems with the profile shape could arise from dropsondes not being a true vertical profile, but instead advecting horizontally through multiple regimes downwind and around the storm. For example, in very high wind speed profiles, dropsondes can commonly pass in or out of the eyewall and translate downwind 20°–30° azimuthally, although this rarely happens close to the surface. Another possible shape issue is caused by the presence of a strong gust or outflow from intense rain. Such gusts can occur at any wind speed, storm intensity level, or sector. When present, a strong gust will cause an individual dropsonde profile to not be representative of a mean profile. A common example of profiles that are suspect, but included in our analysis, is shown in Fig. 3. Examples like this are rare for wind speeds below 25 m s^{-1}, but are quite common for wind speeds > 35 m s^{-1}. It has also been suggested (H. Vömel 2021, personal communication) that they are

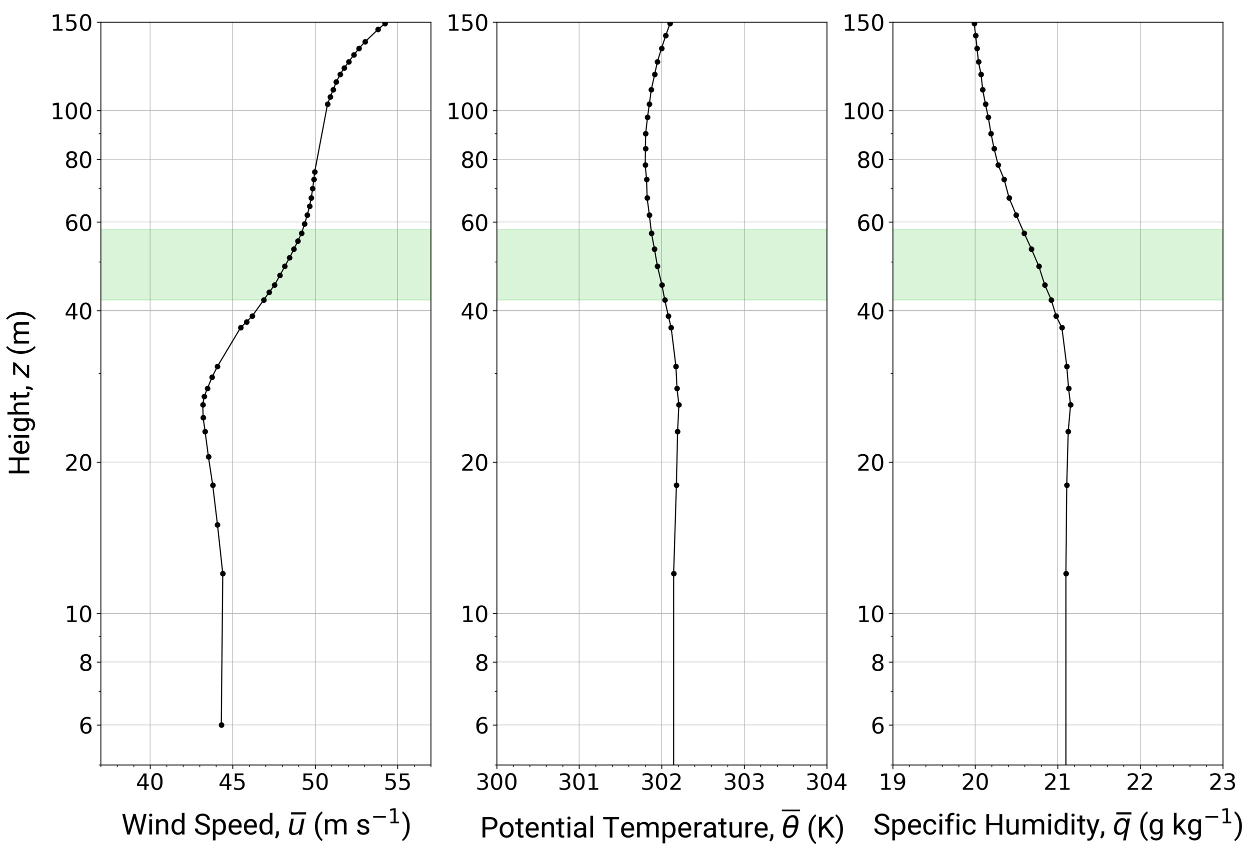

FIG. 3. Vertical profiles from dropsonde D20201006_114554 launched by NOAA42 into Hurricane Delta on 6 Oct 2020. The log-like layer is highlighted in green.

artifacts of errors in the height of dropsondes, where the sonde has hit the water surface at a height just below the minimum in wind speed. These profiles support and are good examples of a warning by M. Powell (2000, personal communication) to be cautious about using dropsonde data where the heights are less than 30 m. We address this interpretation in section 5a. Our reselection of dropsondes errs on the side of caution and should be reexamined in future work.

Concern about ASPEN's smoothing

We found that ASPEN's quality control successfully removed data that was inconsistent with surrounding data. Therefore, there are benefits (in addition to corrected heights) for using data processed by ASPEN rather than using raw data. However, there was concern that ASPEN's smoothing might alter (or even prescribe) our results. To assess this concern, we reduced ASPEN's smoothing weight by up to a factor of five, which resulted in much noisier profiles. We examined the impacts of smoothing with dropsondes from flights 20200826H1 in Hurricane Laura and 20201008I1 in Hurricane Delta, both in 2020, totaling 62 dropsondes. After quality control of the output (section 4d), ASPEN's smoothing has no meaningful impact on the results of a log-profile analysis.

4. Methodology

Nonneutral profiles are obtained through a best fit methodology by minimizing the average of squared difference [Eq. (17)] between profiles constrained to match theory [MOST, Eqs. (1)–(3)] and observations for each observation height. This methodology is applied simultaneously for wind speed, potential temperature, and humidity, with the initial guess for the iterative process calculated using neutral stratification. The squared misfit for each of these variables is scaled by the variance of that variable to remove dependence on units and to have roughly similar impact from each variable when they are combined into a sum of misfits [Eq. (17)] which is ideal when solving for values that minimize the misfits for multiple terms. If one of these variances is zero, that variable is excluded from this calculation and the corresponding values of u_*, θ_*, and q_* are set to zero (consistent with zero vertical shear):

$$\text{misfit} = \frac{\sum_{i=1}^{N_{\overline{u}}}(\overline{u}_i - \overline{u}_{\text{obs}_i})^2}{N_{\overline{u}}\sigma^2_{\overline{u}_{\text{obs}}}} + \frac{\sum_{i=1}^{N_{\overline{\theta}}}(\overline{\theta}_i - \overline{\theta}_{\text{obs}_i})^2}{N_{\overline{\theta}}\sigma^2_{\overline{\theta}_{\text{obs}}}} + \frac{\sum_{i=1}^{N_{\overline{q}}}(\overline{q}_i - \overline{q}_{\text{obs}_i})^2}{N_{\overline{q}}\sigma^2_{\overline{q}_{\text{obs}}}}, \tag{17}$$

where $N_{\overline{u}}$, $N_{\overline{\theta}}$, and $N_{\overline{q}}$ are the number of observations in the log layer for wind speed, potential temperature, and humidity, respectively.

A conjugate gradient method is used to solve the above equation combined with theoretical descriptions of the profiles described in section 2. Most conjugate gradient methods require derivatives of the functional [i.e., the misfit, Eq. (17)] with respect to each of the variables being solved, which is quite awkward when boundary layer stratification is considered. We applied the Powell method (Powell 1964) to solve for our log-profile parameters because it has the advantage of not requiring the explicit solution of derivatives of the function being minimized. Specifically, we used the subroutine optimize.minimize() from the SciPy Python library (Virtanen et al. 2020).

a. *Mismatch between dropsonde data and Monin–Obukhov similarity theory*

A single dropsonde does not provide sufficient sampling to determine mean vertical profiles of wind, temperature, and humidity. Unadjusted dropsonde data show a great deal of observation-to-observation variability because they are influenced by individual eddies. Furthermore, strong precipitation could impact velocities, temperatures, and humidities in a manner inconsistent with MOST. Prior studies (Powell et al. 2003; Holthuijsen et al. 2012; Richter et al. 2021) have addressed this problem by compositing profiles with similar near-surface wind speeds. This approach assumes that 1) roughness length is purely a function of winds speed (ignoring sea state) and storm relative location, 2) atmospheric stratification is close to neutral, and 3) displacement height is small. Previous work on composite dropsonde profiles shows a mean log layer extending several hundred meters into the boundary layer (Franklin et al. 2003; Powell et al. 2003).

Our approach is to determine the log profiles, constrained to follow the MOST, that are best fits to individual dropsonde observations. Rather than attempting to smooth individual profiles of observations, we attempt to find the best fit to profiles that are forced to be consistent with MOST. This is loosely analogous to the WL150 estimate of $\overline{u}_{10}$, which uses data from a layer 150 m thick to make this estimate. This approach relies on the following assumptions.

1) The solutions can be a noisy estimate of an appropriately sampled profile.
2) Our quality control methods can distinguish between useful (good) matches to dropsonde data and poor matches.
3) Our quality control methods are not too restrictive. They do not limit the results in a manner that prescribes the outcome.
4) The ensemble of noisy results provides a measure of central tendency (such as a mean, median, or mode) that is insightful (e.g., shows a dependency or lack of dependency on wind speed).
5) The layer to analyze can be identified sufficiently often.

The first requirement does not require that dropsonde data are an approximate match to a mean profile; however, the second requirement could do so if log-profile parameters are limited to be near expectations. Hence, the third requirement is needed to avoid prescribing results. We must allow solutions to span a much wider range of parameter space than expected. Since individual solutions might be quite noisy (we will show this is the case), like prior studies, we must apply some filtering to examine dependencies. Our approach has the advantage of being able to address substantial variability in displacement heights, stability, and roughness length which

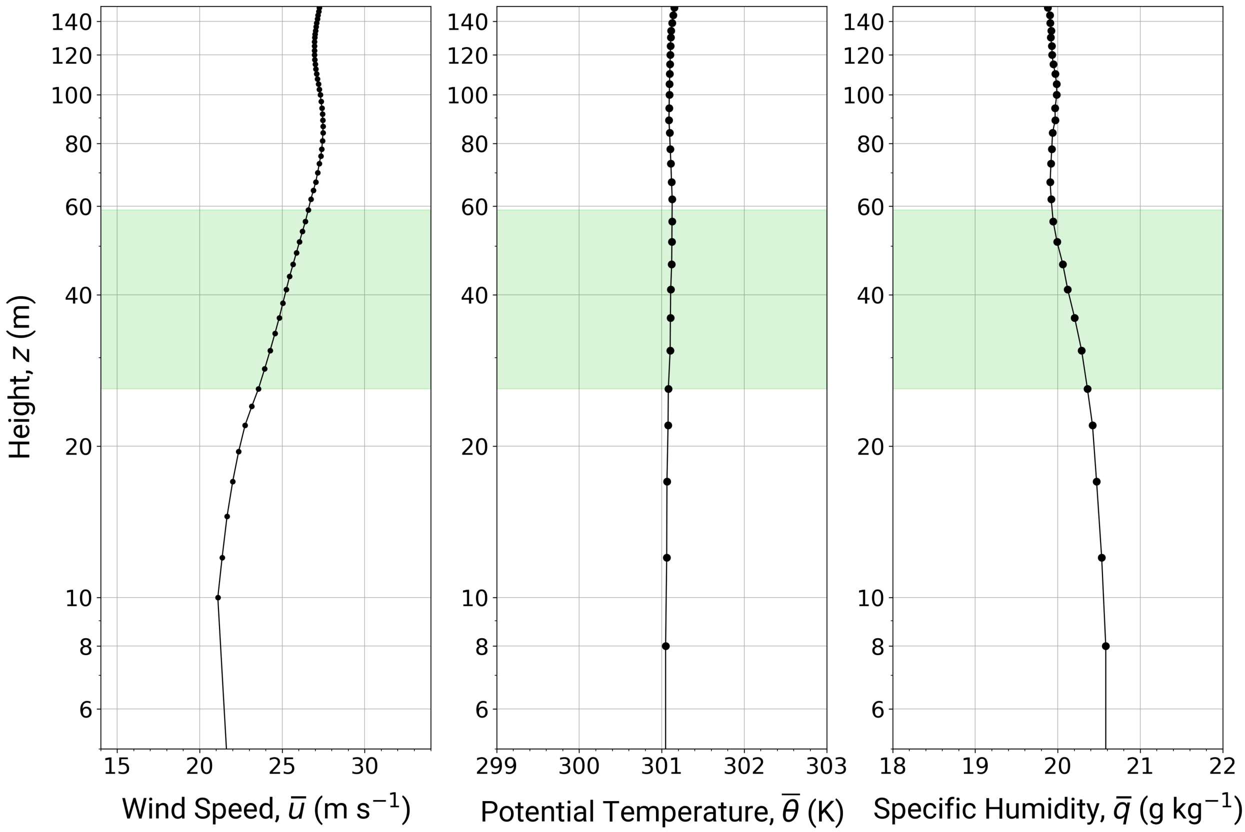

FIG. 4. Log layer (green shading) identified for dropsonde D20201007_134320 dropped by NOAA42 into Hurricane Delta on 7 Oct 2020. The horizontal axes are (left) wind speed, (center) potential temperature, and (right) specific humidity.

would be linked to issues with dropsondes and to natural variability in surface fluxes and transfer coefficients.

The greatest weakness of our current approach is that the layer to be examined was estimated by a student who 1) visually selected layers that had roughly linear features when plotted as a function $\ln(z - d)$ and 2) made small adjustments after accounting for displacement height. Identification of these layers is described in more detail in the methodology (section 4e). This limitation is why we consider this study a proof of concept. Broader application of this profile analysis technique would greatly benefit from automation of the selection of heights covered by the log layer (Fig. 4).

b. Determining log-profile parameters

The variables used to parameterize these profiles can be thought of as fitting parameters: u_*, θ_*, q_*, d, the natural logs of each of the roughness lengths, and the values to which the profiles extrapolate at $z = d$. Parameters that have positive and negative bounds that exceed the range of plausible values [e.g., $\ln(z_0)$ rather than z_0] are easiest to work with. Errors in the assumption that the value of a profile extrapolated to $z = d$ is equal to the value at $z = 0$ are amplified exponentially in the solution's roughness lengths, resulting in relatively noisy roughness lengths. Without better in situ measurement of the surface (i.e., at the displacement height), the next best option was to treat the surface values as unknowns and solve for them in the same manner we solve the other profile parameters. A minor downside of this approach is that it requires observations at an additional height in each log profile.

c. Initial guesses

The initial guesses for the log-profile fitting parameters are determined from the solutions to fits of the neutral equations ($\Psi = 0$), with the surface values set to the dropsonde's surface values (and $\overline{u}_d = 0$ m s^{-1}). Neutral or near-neutral conditions ($\sim -0.07 < z/L < +0.005$; Stopa et al. 2022) have been common assumptions in the context of tropical cyclone boundary layers (e.g., Powell et al. 2003). The stratification term (Ψ), as previously mentioned, is a function of the height divided by the Obukhov length (z/L). The z/L is proportional to the ratio of turbulent kinetic energy (TKE) production by buoyancy to TKE generated by wind shear instabilities. In TC conditions, the shear stress is much larger than the buoyancy flux, which means the magnitude of z/L is small and the magnitude of Ψ is small (regardless of parameterization). This situation suggests that a neutral profile ($\Psi = 0$) will often be a good approximation. The initial guess uses a surface $\overline{q}$ that is calculated using the observed dropsonde temperature at $z = d$, the highest observed dropsonde pressure, and an estimated sea surface RH of 98%, which is reduced from 100% due to salt in the water

TABLE 3. Lower and upper bounds are chosen for minimization function. The subscript d represents the profile values at the height $z = d$. The LB indicates the height of the lower boundary of the log layer. The values inside the natural logs have units of meters.

Unknown	Search bounds	Unknown	Search bounds
u_*	0.1, 6.0 m s^{-1}	$\overline{u}_d$	$u_{\mathrm{sfc}_0} \pm 3.5$ m s^{-1}
θ_*	−0.5, 0.5 K	$\overline{\theta}_d$	$\theta_{\mathrm{sfc}_0} \pm 3.5$ K
q_*	−0.5, 0.5 g kg^{-1}	$\overline{q}_d$	$q_{\mathrm{sfc}_0} \pm 2.5$ g kg^{-1}
d	−15, LB m	$\ln(z_0)$	$\ln(10^{-8})$, $\ln(10)$
$\ln(z_{0\theta})$	$\ln(10^{-8})$, $\ln(10)$	$\ln(z_{0q})$	$\ln(10^{-8})$, $\ln(10)$

(Feistel et al. 2010). A consequence of this approach is that all three profiles can be treated as independent. The solutions have negligible sensitivity to first guesses, provided they are not seriously inconsistent with the data.

d. Bounds for solutions and related quality control

To apply this to the profile fitting, it was necessary to set physical bounds for each of the 10 variables being determined (Table 3) and a requirement that these bounds be wide to avoid prescribing results. Solution variables that match one of the search bounds indicate that the conjugate gradient method was trying to find a solution outside the bounds and that the solution is unlikely to be a good fit to the data for that variable. The variable flagged as matching this bound is almost always a roughness length. This occurs despite bounds being set to a very large span to avoid flagging too large a fraction of the data. However, this approach does mean that the roughness lengths should be used with caution. These bounds are listed in Table 3. At least one limit is matched for 122 wind profiles, 137 temperature profiles, and 198 moisture profiles from the batch of 387 dropsondes that we processed.

e. Identification of the log-like layers

MOST analysis methods assume that the data used in the analysis are from within the log layer (also called the constant flux layer, referring to near-surface vertical turbulent fluxes), which is typically defined as above a roughness layer and below an Ekman layer. The roughness layer is found between the surface and the constant flux layer. Roughness layers occur due to airflow around, between and over roughness elements (i.e., the structures making the surface rough: e.g., crops, forests, buildings, or waves). In TCs, surface waves can be quite large (10 m or more) (Wright et al. 2001; PopStefanija et al. 2021; Walsh et al. 2021), but the roughness layer over water is only a fraction of this height (Bourassa et al. 1999). Hypothetically, a spray layer or flow over waves could cause an extension of the roughness layer. In 15% of the dropsonde profiles, e.g., the example in Fig. 2, we exclude data from >10 m below a log-like layer.

The upper extent of a log-like layer can be difficult to identify in cases that smoothly transition from a log layer. This kind of problem is shown clearly in analyses of wave tank mean winds (Bourassa et al. 1999). Our methodology does not require data from the whole log-profile region. It converges on a good fit to the data provided there are enough data in the log layer being examined and provided the profiles are not too large a departure from MOST. We are cautious to avoid including data from above the log layer. Identification of the upper boundary, and particularly the lower boundary, benefits from repeated use of the analysis code to evaluate layers (in part due to changing displacement heights and stratification) and the sensitivity of the best-fit profiles to these parameters. This manual determination of the vertical bounds of log layers is very tedious and time consuming. The time involved in identifying log layers was the limiting factor in the number of dropsondes we processed. Future developments should include automation of this process.

We found that for wind speeds < 20 m s^{-1} we needed a thicker boundary layer to reduce noise in our results. Rather than requiring data from at least four heights, requiring data from at least seven heights greatly reduced the scatter. For greater wind speeds, an increase in the requirement has insignificant impact, other than to reduce the number of our solutions.

Log layers that we identified within individual dropsonde profiles are not nearly as thick as layers found in studies that binned dropsondes. This difference in characteristics could be related to dropsondes' poor sampling of a mean combined with increasing space and time scales of eddies further from the surface. Automated identification of the TC boundary layer will likely be required to further examine the upper bound of a log layer; thus, we do not pursue this question herein.

5. Results and discussion

Our methodology determines values for boundary layer variables consistent with the best fit to dropsonde profiles in a selected log layer near the surface. These best-fit profiles are used to estimate near-surface (i.e., 10 m above the displacement height) values of wind speed, temperature, and humidity. Surface fluxes [Eqs. (11)–(13)] can also be calculated as products of the dimensional scaling parameters (u_*, θ_*, q_*) without the underlying assumption of a transfer coefficient or roughness length dependency on friction velocity. Example output (Fig. 5) shows the calculated profiles plotted over the dropsonde data, and it displays the boundary layer parameters, extrapolated near-surface values, and calculated fluxes. The near-surface wind speed, temperature, and humidity can be combined with the dimensional scaling parameters to determine transfer coefficients [Eqs. (14)–(16)]. We largely focus on measures of central tendency as a function of wind speed because of the noise in individual observations. In the following sections, we will first examine parameters related to our assumptions about displacement height (section 5a) and stratification (section 5b) and then demonstrate that 1) the surface wind speeds are similar to NOAA estimates of these winds (section 5c), 2) the median drag coefficient for wind speeds from 10 to 20 m s^{-1} is a good match to well-known in situ values (section 5d), and 3) that our median C_D has a dependence on near-surface wind speed that is qualitatively similar to prior observations (section 5d). These findings help

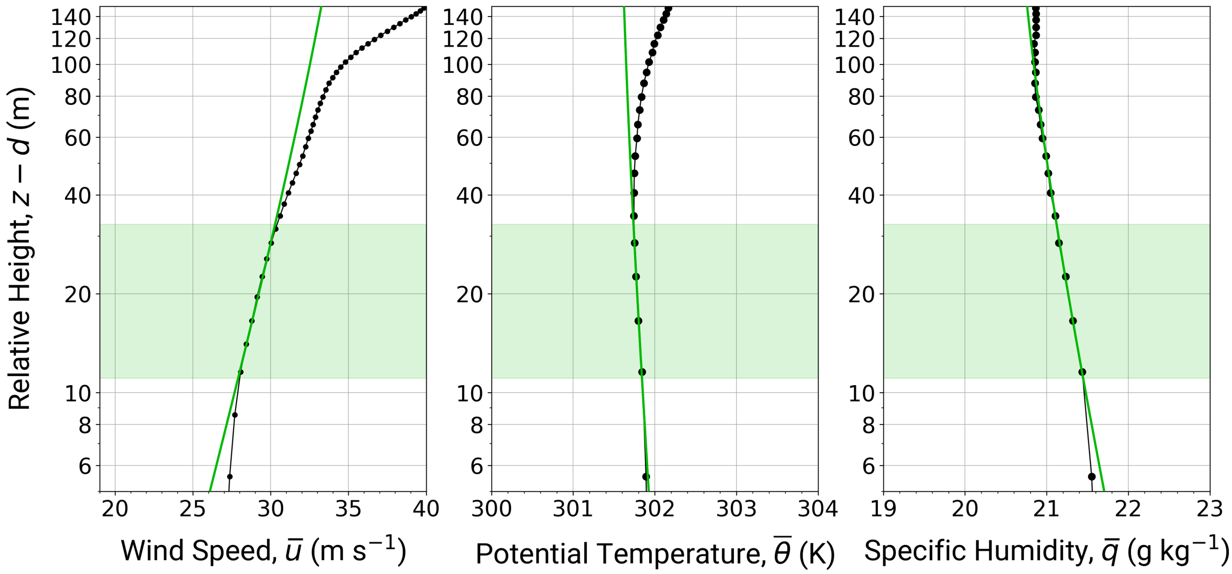

d = 17.5 m	$\bar{u}_d$ = -0.88 m s^{-1}	$\bar{\theta}_d$ = 302.54 K	$\bar{q}_d$ = 26.30 g kg^{-1}
Stability (z/L) -9.90E-04	u_* = 0.9420	θ_* = -0.04407945	q_* = -0.00013784
	$\bar{u}_{10}$ = 27.68 m s^{-1}	$\bar{\theta}_{10}$ = 301.85 K	$\bar{q}_{10}$ = 21.48 g kg^{-1}
WL150$_{10}$ 27.0 m s^{-1}	τ = 1.000 N m^{-2}	Q_{sen} = 47.067 W m^{-2}	Q_{lat} = 366.026 W m^{-2}
	C_D = 1.158 x 10^{-3}	C_H = 2.190 x 10^{-3}	C_E = 1.033 x 10^{-3}

FIG. 5. Solution profile (green lines) calculated for the selected log layer (shaded) selected from dropsonde D20201007_043433 (black dots) launched into Hurricane Delta by NOAA43 on 7 Oct 2020. All heights are relative to d. Variables in profile parameterizations [Eqs. (1)–(3)], extrapolated 10-m values, and calculated fluxes are listed below the profile graphics. The surface-reduced WL150 wind speed is shown in comparison to the extrapolated 10-m wind.

provide confidence in our results. Results are also presented for surface turbulent fluxes (section 5e).

a. *Displacement height*

One of the motivations for developing our methodology was that displacement height could be substantial in a storm and would likely depend on wave characteristics as well as wind. Over the ocean, a displacement height due to waves (d) is no more than 80% of the significant wave height (Bourassa 2006) and is normally treated as zero over water. Prior studies have treated displacement height as negligibly small. Another motivation was that errors in estimation of the surface can be removed through inclusion in displacement height.

A scatterplot of displacement heights as a function of wind speed (Fig. 6) shows a great deal of scatter. Scatter is expected to be due to the relatively poor characteristics of dropsonde observations for our fits to log profiles and due to errors in the estimation of the surface. Some of this variability could also be due to natural processes that vary throughout storms (e.g., sea state). A rolling bin system is used to calculate statistics (median and uncertainty in a mean), where the lower boundary of the lowest wind speed is $\bar{u}_{10} - \bar{u}_d = 11$. The bin width starts at 8 m s^{-1} for the lowest wind speed values and incrementally increases linearly up to a maximum of 20 m s^{-1} when the lower bound is 54 m s^{-1}. The blue solid line represents the median value at each bin center. The blue dashed lines represent the uncertainty in the mean (i.e., standard error), defined as ±1 standard deviation divided by the square root of the number of data points within the bin ($\pm 1\sigma/\sqrt{N}$). This uncertainty includes random errors in our solution, geophysical variability due to factors other than wind speed, and errors in the estimation of the surface. Lighter shading, regardless of color, represents the 10th–90th percentiles. Darker shading, regardless of color, represents the 25th–75th percentiles (quartiles). Blue color shading represents bins with 28 or more data points (a continuous region of more confidence), indicating relatively high confidence. Gray color shading represents bins with fewer than 28 data points, indicating relatively low confidence.

The distribution of our displacement heights shows a dependency on wind speed (Fig. 6): The median displacement increases as wind speed increases. This figure confirms the approximately 5-m random error and confirms the systematic response suggested by H. Vömel (2021, personal communication) and Richter et al. (2021), but it cannot determine if the systematic response is an error. The large median value and trend are tantalizing signs that another process could be coming into play for wind speeds > 25 m s^{-1}. Regardless of the interpretation, these results suggest that there is merit in methods that account for nonzero displacement heights.

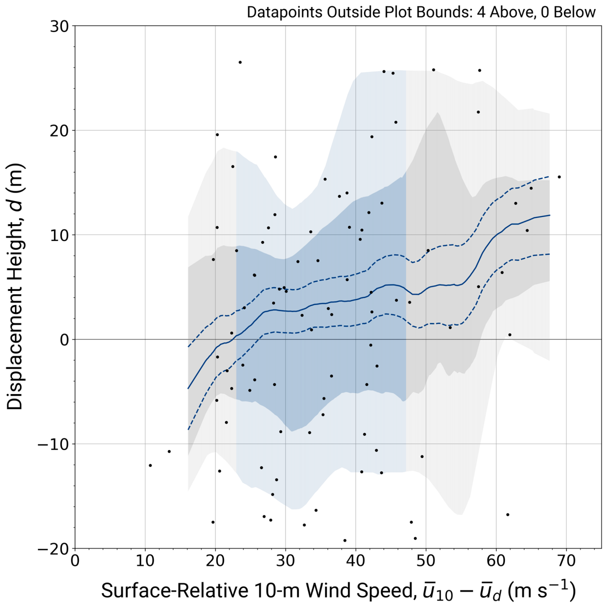

FIG. 6. Displacement heights as a function of wind speed. The scatterplot is statistically analyzed using a rolling bin system. The solid blue line represents the median at bin centers. The blue dashed lines represent uncertainty in the mean (±1 standard deviations divided by the square root of the number of data points within the bin). Regardless of color, darker shading represents the 25th–75th quartiles, and lighter shading represents the 10th–90th percentiles. Blue shading represents bins with 28 or more data points and an acceptable level of confidence. Gray shading indicates fewer than 28 points per bin and relatively low confidence. For wind speeds below 35 m s^{-1}, there is a small positive mean combined with a random distribution. For wind speeds > 40 m s^{-1}, there is a stronger tendency for positive values.

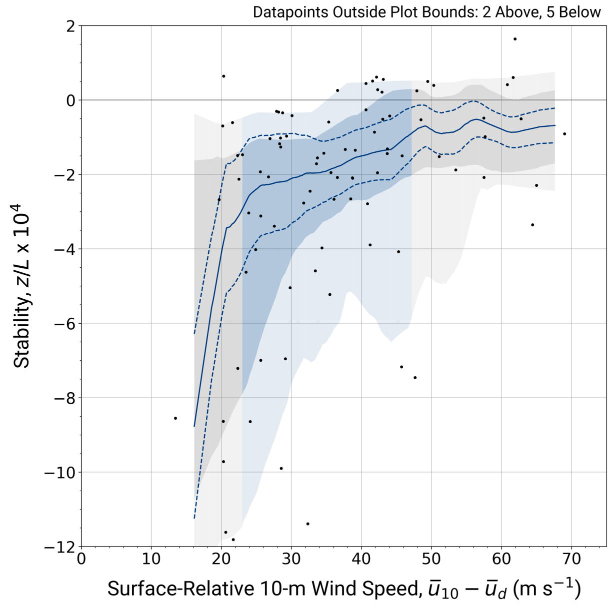

FIG. 7. Dimensionless Obukhov length scale as a function of wind speed. This plot demonstrates that stratification is usually slightly unstable ($\Psi < 0$) rather than neutral ($\Psi = 0$) for TC conditions. Binning, formatting, and statistics follow the descriptions of Fig. 6.

If the systematic increase in displacement height with increasing wind speed is not due to systematic errors in assigning (or defining) the surface height from dropsonde data, this increase might be due to a spray layer (Andreas 1992; Andreas et al. 1995; Andreas and Emanuel 2001). Previous studies have suggested that these layers of spray have a friction-reduction effect and should reduce both the drag coefficient and stress (Andreas and Emanuel 2001; Emanuel 2018; Troitskaya et al. 2019), which is qualitatively consistent with our Figs. 9 and 11a. In concept, momentum lost to spray is extracted from the stress that contributes to wave-induced surface roughness (z_0). Consequently, there is a change in the balance between surface wind speed, stress, and roughness length. Further analysis with boundary layer profiles combined with surface stress estimates from in situ platforms like uncrewed surface vehicles (USVs) or aerial systems (UASs) could be helpful to improve our understanding of these processes and interpret the cause of the displacement height dependency on wind speed.

b. Boundary layer stratification

Near-neutral conditions ($\sim -0.07 < z/L < +0.005$; Stopa et al. 2022) have been approximated as neutral in the context of TCs (e.g., Powell et al. 2003). This study is the first demonstration of this expected result: almost all the values of z/L calculated from dropsonde data fall in the range of near-neutral conditions (Fig. 7). Most of the calculations for stratification are negative, indicating slightly unstable conditions. This is to be expected from a boundary layer that is warmed from below. This finding supports the approximation of near-neutral stratification in prior studies and indicates that surface turbulent fluxes and transfer coefficients are slightly larger than if they were calculated assuming neutral conditions.

c. The 10-m wind speed

An important output of this methodology is the 10-m wind, $\bar{u}_{10}$, which is used to calibrate airborne remote sensors for measuring surface winds in TCs, and the airborne instruments are in turn used to calibrate satellite observations. Our calculation applies Eq. (1), for the best-fit log-layer profile, where $z - d = 10$ is a height of 10 m above the displacement height d. The currently favored approach to estimating a 10-m wind from dropsonde data is the surface-reduced WL150 (WL150$_{10}$) which, as discussed in the introduction, is a layer mean of the lowest 150 m of dropsonde wind data with a reduction coefficient applied to account for the height of this layer (Uhlhorn et al. 2007; Franklin et al. 2003). To compare the two methodologies, a scatterplot is shown in Fig. 8. There is substantial variance throughout, increasing as wind speed increases. These show an excellent fit of WL150$_{10}$ relative to our $\bar{u}_{10}$ from 20 to 35 m s^{-1} and an overestimation of WL150$_{10}$ relative to our $\bar{u}_{10}$ from 35 to 50 m s^{-1}. It should be noted that WL150$_{10}$ is at height $z = 10$, whereas our methodology is at height $z = d + 10$. The similarity of the two methodologies is encouraging, but cannot be treated as proof our methodology works.

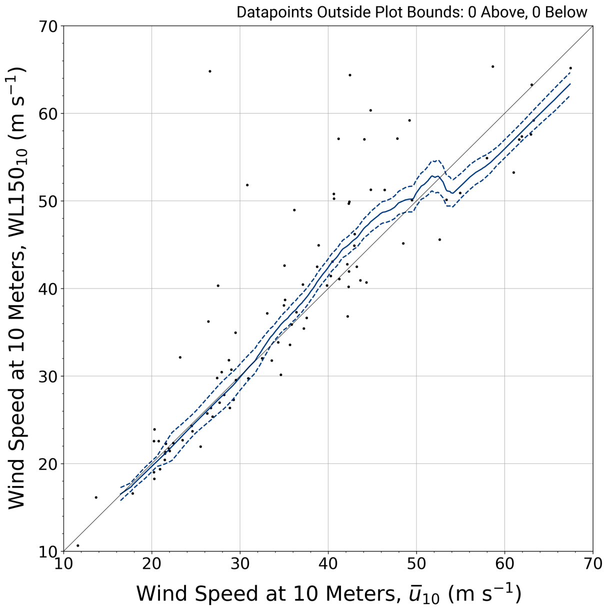

FIG. 8. Surface-reduced WL150 vs log-layer extrapolated 10-m wind speed for all dropsonde profiles analyzed. The solid blue line is the median $\overline{u}_{10}$ from the WL150 method vs the median $\overline{u}_{10}$ from the dropsondes; the blue dashed lines represent dropsonde $\overline{u}_{10} \pm 1$ standard deviation uncertainty in the mean difference. All statistics calculated by rolling bins in steps of 0.1 m s^{-1} with bin widths starting at 8 m s^{-1} and increasing linearly across the range up to 20 m s^{-1}.

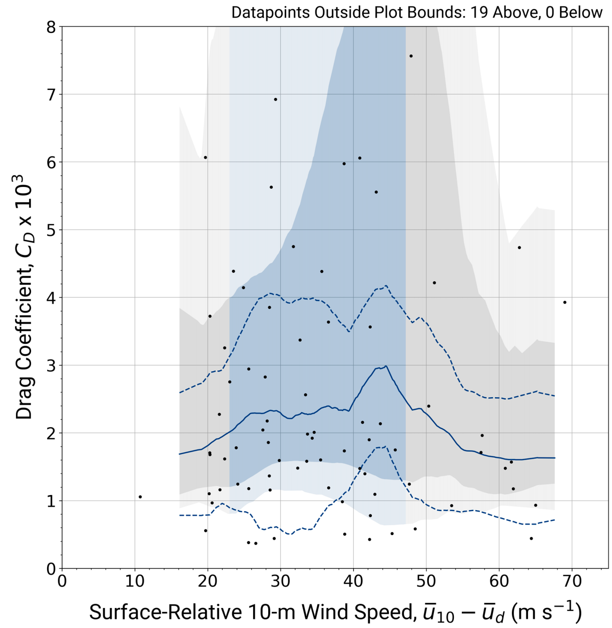

FIG. 9. Drag coefficient as a function of wind speed. Binning, formatting, and statistics follow the descriptions of Fig. 6.

d. Drag coefficient

Our drag coefficients are shown in Fig. 9. A comparison of results with this current methodology to those of some past studies is depicted in Fig. 10. The median drag coefficients for 10–20 m s^{-1} wind speeds are consistent with well-tested in situ observations. This match is notably better than prior studies (Powell et al. 2003; Holthuijsen et al. 2012; Richter et al. 2021), suggesting (but not confirming) a strength of the profile analysis presented herein. However, the wide error bars prevent this speculation from being confirmed. Speculatively, our use of displacement height to adjust the profiles to a common surface height seems most likely to be responsible for this difference in results.

It is interesting to note that the peaks in the quartiles occur at similar wind speeds as the cross-swell front left sector data from both studies shown (Powell 2006; Holthuijsen et al. 2012; Fig. 10b). We have too few samples to evaluate for differences in sector averages. The uncertainty in C_D is too great to confirm that C_D drops for extreme winds as suggested by previous studies (Powell et al. 2003; Holthuijsen et al. 2012; Richter et al. 2021).

e. Turbulent fluxes of momentum, sensible heat, and latent heat

Panels of the three turbulent fluxes mentioned are shown in Fig. 11. The stress (Fig. 11a), sensible heat flux (Fig. 11b), and latent heat fluxes (Fig. 11c) each steadily increase with wind speed, possibly saturating for wind speeds around 40–45 m s^{-1}. The error bars become quite large for wind speeds above this range. There are 17, 13, and 16 values of stress, sensible heat flux, and latent heat flux, respectively, that exceed the range of values shown in Fig. 11. Despite a median having little sensitivity to outliers, the fact that most of these outliers are larger than the median suggests a skewed error distribution that could include a positive bias. Most of these outliers are associated with roughness lengths that are much larger than the roughness lengths for fluxes near the medians.

The densest cluster of latent heat fluxes as a function of wind speed has values that are similar to spray-modified fluxes, as discussed by Yang et al. (2024, 2025). Larger sensible heat fluxes would have been a better indicator of sea spray modifying fluxes. Sensible heat flux values at the 75th percentile are similar to the wind speed dependency of spray-mediated fluxes found by Yang et al. (2024, 2025) for $\overline{u}_{10} < 45$ m s^{-1}. Our sampling for $\overline{u}_{10} > 45$ m s^{-1} is too sparse and too uncertain to draw conclusions about changes in the dependency on wind speed, and the rolling bin size for wind speeds extends this problem down to $\overline{u}_{10} > 35$ m s^{-1} for the median and uncertainties. Reduced uncertainty in the medians or enough observations to support cluster analysis would likely be needed to confidently assess the hypothesis that spray enhances sensible and latent heat fluxes as suggested by Andreas and Emanuel (2001).

6. Conclusions

We have developed a methodology to determine log-profile parameters and fluxes based on MOST profiles that are best fits to dropsonde-based data for wind speed, potential

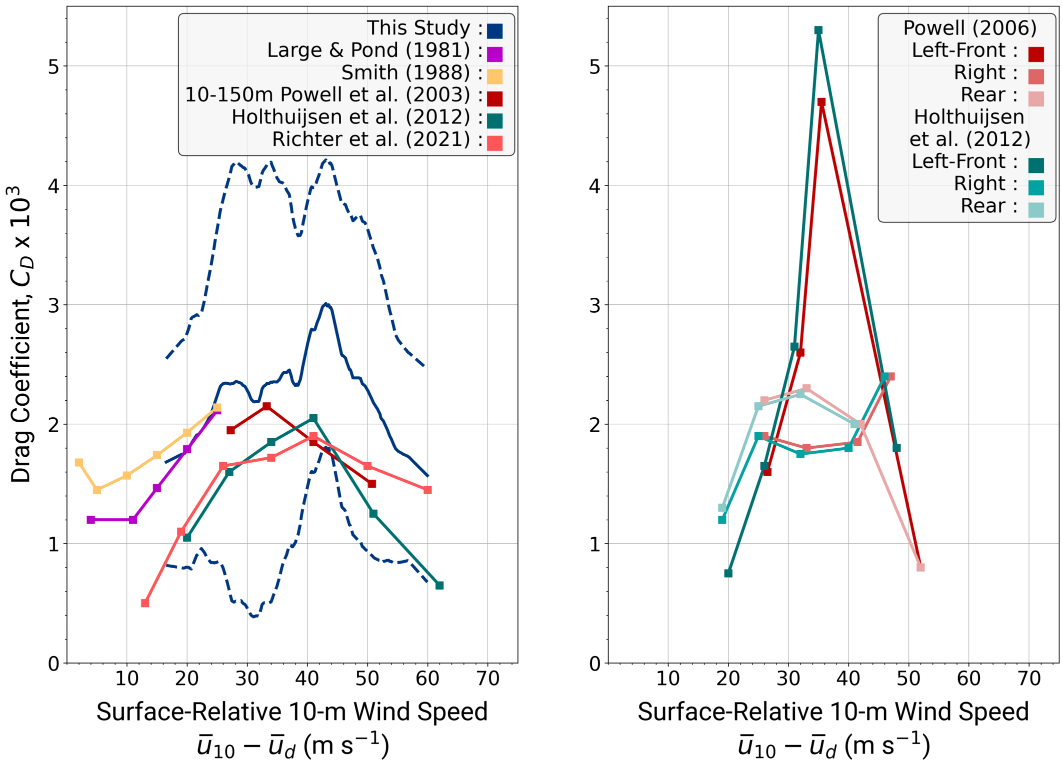

FIG. 10. (left) A comparison of median binned drag coefficients from this study (blue solid line) with other published values (Large and Pond 1981; Smith 1988; Powell et al. 2003; Holthuijsen et al. 2012; Richter et al. 2021). The dashed blue lines show the uncertainty in the mean (±1 standard deviation divided by the square root of the number of data points within the bin). (right) Comparison to studies broken down by storm sector (Powell 2006; Holthuijsen et al. 2012).

temperature, and specific humidity. This methodology enables us to determine log-profile parameters for each dropsonde that are a sufficiently close match to MOST (10.4% of cases we examined; 25% of those that had data near the surface), albeit with considerable uncertainty. A dropsonde's poor temporal sampling combined with natural variability within a TC environment causes the poor match to MOST and causes substantial fractions of unexplained variability in our estimated log-profile parameters. The methodology is shown to work in all azimuthal sectors for TC intensities ranging from tropical storm to category 5 hurricane. A weakness of this technique applied to dropsonde data is a very large relative uncertainty in the roughness length for each profile variable. Medians are used to examine how boundary layer variables change with wind speed. Across all wind speeds, strong eddy motions and presumably gusts from precipitation can distort the wind profile, and when they are present, individual dropsonde profiles can be so nonrepresentative of a mean profile as to prevent physically plausible solutions. The findings herein demonstrate our approach applied to data from dropsondes in TCs. This is far from an ideal application, but does provide a method for obtaining boundary layer parameters in a TC environment. An approach to smoothing dropsonde data developed by R. Foster (2019, personal communication) has shown that large changes in values for neighboring heights can often be accounted for (assuming the changes are due to eddies). Applying such a technique could increase the number of usable cases and reduce the noise in our results. Another weakness of this methodology is that the layer to be examined is determined subjectively. Future applications of this technique would likely benefit from exploration of methods to reduce this uncertainty as well as automated selection of the log layers. The methodology should work much better for observations that produce more accurate mean profiles.

One of our main goals is to help improve the understanding and dropsonde-based estimation of surface wind speeds in TCs. While more work could be done to reduce uncertainty of our methodology, we can argue that it follows the physics of the near-surface layer better than the more statistically based WL150 because our solutions are constrained to follow MOST and account for displacement height. On the other hand, WL150's average over heights reduces errors associated with undersampling profiles. For $\overline{u}_{10} < 25$ m s^{-1}, modest systematic differences speak well for both techniques. For $25 > \overline{u}_{10} > 50$ m s^{-1}, WL150 overestimates our estimated 10-m winds by 2–3 m s^{-1}. These differences are likely in part due to the small number of profiles available when the WL150 methodology was developed. This difference could also be due to the subsampling needed for our methodology to produce

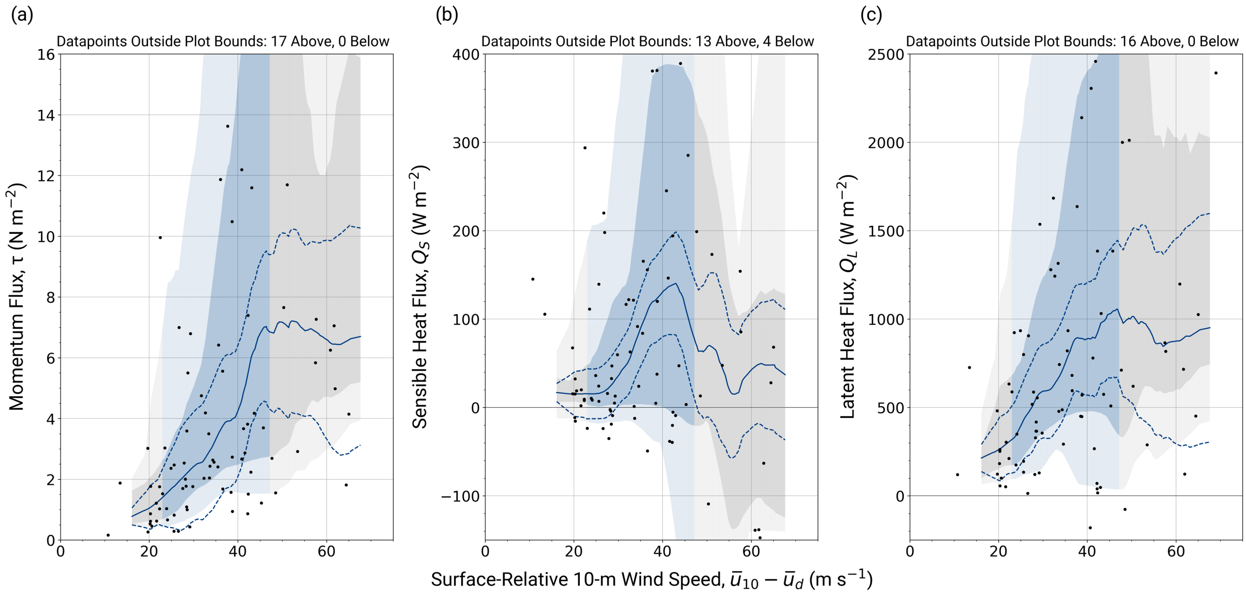

FIG. 11. (a) Stress (momentum flux), (b) sensible heat flux, and (c) latent heat flux, all as functions of the 10-m wind speed relative to the wind speed at d. Binning, formatting, and statistics follow the descriptions of Fig. 6.

solutions. A key conceptual difference between these methodologies is that our estimate of $\overline{u}_{10}$ considers displacement height, which is a vertical offset of the log profile. We found large and seemingly random variability in individual dropsonde profiles, however, the median displacement height (a vertical offset of the base of the log layer) increased as wind speed increased, suggesting that waves, sea spray, or something else was causing this trend in vertical displacement.

Another goal is to estimate turbulent fluxes in TC conditions since most in situ flux measurement instruments are aboard ships and aircraft that rarely enter the boundary layer of a TC. By finding the MOST profiles that are best fits to the observations, we are able to produce these fluxes in a manner that does not assume neutral boundary layer stratification. Our analysis finds that for $\overline{u}_{10} < 40$ m s^{-1}, the boundary layer stratification is usually unstable and within the category of near-neutral conditions Stopa et al. (2022). The slope of the median of the drag coefficient, C_D, agrees well with other observations (Large and Pond 1981; Smith 1988) for wind speeds at which those parameterizations apply, however, the uncertainty in our results is too large to confidently say our C_D is different from prior studies.

The dependencies of turbulent heat fluxes and displacement height on wind speed provided hints of the spray-induced increases in these fluxes found by Yang et al. (2024, 2025) that might be linked to this trend in vertical offset; however, dropsonde observations do not provide enough information to determine the cause of this vertical offset. Observations from a UAS or USV might be able to provide direct estimates of the fluxes through eddy covariance or a UAS might be able to provide boundary layer profiles with sufficient sampling to use log-profile methods to determine fluxes and test hypotheses about wave-related and spray-related changes in the boundary layer.

The large natural variability of TC wind profiles combined with poor temporal sampling of dropsondes is likely responsible for the large variability in the boundary layer parameters derived by this technique. If so, improved sampling of the boundary layer should reduce uncertainty. Higher percentage of profiles would likely be applicable in the future if new dropsondes (or other probes) would be equipped with sensors capable of obtaining more observations within the log layer and ideally a much slower fall rate in the log layer. Alternatively, if a drone could survive in this environment, it could provide multiple profiles that could be combined to produce better mean profiles.

Acknowledgments. This research is loosely based on the MS thesis work of one of the authors, Daniel Wallace, and part of the MS thesis work of Amelia Bryan, both at Florida State University. It was funded in large part by NASA Physical Oceanography via the Jet Propulsion Laboratory (Contract 1419699 and 5129) and a NASA HQ grant for Ocean Vector Wind Leadership, in part by the Global Ocean Monitoring and Observing Program via the Northern Gulf Institute (NGI; Fund 100007298, NGI Grants 22-NGI4-26, 23-NGI4-56, and NGI4-89), and in part by the U.S. Department of Commerce National Oceanic and Atmospheric Administration through the NGI (Awards NA16OAR4320199 and NA21OAR432-0190). The authors would also like to thank Ralph Foster for his insightful input and critical assessment early in this study, as well as James Franklin, Sim Aberson, Holger Vömel, and three anonymous reviewers who provided extremely helpful comments and suggestions.

Data availability statement. All dropsonde data are available from NOAA/AOML/HRD via https://www.aoml.noaa.gov/hrd/data_sub/dropsonde.html.

APPENDIX

Tables of Variables

Tables A1 and A2 show definitions of all symbols and subscripts, respectively, used herein.

TABLE A1. List of symbols.

Symbol	Name	Units	Description
C_D	Drag coefficient, momentum transfer coefficient	Unitless	Ratio of friction velocity (u_*) squared to wind speed squared
C_P	Heat capacity	J kg^{-1} K^{-1}	Energy required to heat 1 kg or air 1 K
d	Displacement height	m	A vertical offset of the portion of the wind profile representing the log layer
k	Von Kármán constant ≈ 0.4	Unitless	Boundary layer constant
L	Obukhov length (m)	m	z/L represents the ratio of buoyant production (or consumption) of TKE relative to production from wind shear
L_V	Latent heat of vaporization	J kg^{-1}	Energy required to convert 1 kg of water to water vapor
N	No. of observations in the log layer	Unitless	
q	Specific humidity	kg kg^{-1}	Ratio of mass of water vapor in 1 kg of air to the mass of the air.
q_*	No common simple name	kg kg^{-1}	Nondimensionalizing scale (kg kg^{-1}) for the difference in mean specific humidity between height z and the displacement height (d)
Q_{lat}	Latent heat flux	W m^{-2} s^{-1}	Upward flux density of energy stored as water vapor
Q_{lat}	Sensible heat flux	W m^{-2} s^{-1}	Upward flux density of energy stored as heat without change of phase
u	Horizontal wind speed	m s^{-1}	Horizontal wind speed in the vector mean wind direction
u_*	Friction velocity	m s^{-1}	Nondimensionalizing scale for the difference in mean wind speed between height z and the displacement height (d)
z	Height	m	Height above the surface. Surface is not clearly defined, but this variable is used in the form $z - d$, where d is relative to the same ill-defined surface.
z_0	Roughness length	m	Displacement height (m): a vertical offset of the portion of the wind profile representing the log layer
θ	Potential temperature	K	Temperature of air if it were moved to a standard pressure level due to changes in volume without changes in phase
θ_*	No common simple name	K	Nondimensionalizing scale (K) for the difference in mean potential temperature between height z and the displacement height (d)
Ψ	Stratification term is modified log-profile equations	Unitless	The vertical integration of the impact of stratification on vertical shear
ζ	No common simple term	Unitless	Variable for collecting simplifying variables in Ψ
ρ	Air density	kg m^{-3}	Density of moist air at height d
σ	Standard deviation		
τ	Stress	N m^{-2}	Downward flux density of horizontal momentum

TABLE A2. Definition of subscripts.

Subscript	Description
i	Indicates values are from a particular level. The value of i is the index for that level
D	Indicates the value is from the extrapolation of the log profile to the lower boundary of the layer at the displacement height or surface if $d = 0$
10	Indicates the value is from 10 m above the displacement height
obs	Indicates observational data
u, θ, and q	A subscript indicating association with wind speed, temperature, and humidity profile, respectively
M, H, or E	A subscribe indicating association with momentum, sensible heat, or moisture, respectively
sfc_0	Value at the surface provided in the dropsonde data

REFERENCES

Ahern, K., M. A. Bourassa, R. E. Hart, J. A. Zhang, and R. F. Rogers, 2019: Observed kinematic and thermodynamic structure in the hurricane boundary layer during intensity change. *Mon. Wea. Rev.*, **147**, 2765–2785, https://doi.org/10.1175/MWR-D-18-0380.1.

Andreas, E. L., 1992: Sea spray and the turbulent air-sea heat fluxes. *J. Geophys. Res.*, **97**, 11 429–11 441, https://doi.org/10.1029/92JC00876.

——, and K. A. Emanuel, 2001: Effects of sea spray on tropical cyclone intensity. *J. Atmos. Sci.*, **58**, 3741–3751, https://doi.org/10.1175/1520-0469(2001)058<3741:EOSSOT>2.0.CO;2.

——, J. B. Edson, E. C. Monahan, M. P. Rouault, and S. D. Smith, 1995: The spray contribution to net evaporation from the sea: A review of recent progress. *Bound.-Layer Meteor.*, **72**, 3–52, https://doi.org/10.1007/BF00712389.

Beljaars, A. C. M., and A. A M. Holtslag, 1991: Flux parameterization over land surfaces for atmospheric models. *J. Appl. Meteor.*, **30**, 327–341, https://doi.org/10.1175/1520-0450(1991)030<0327:FPOLSF>2.0.CO;2.

Bender, L. C., N. L. Guinasso, J. N. Walpert, and S. D. Howden, 2010: A comparison of methods for determining significant wave heights—Applied to a 3-m discus buoy during Hurricane Katrina. *J. Atmos. Oceanic Technol.*, **27**, 1012–1028, https://doi.org/10.1175/2010JTECHO724.1.

Black, P. G., and Coauthors, 2007: Air–sea exchange in hurricanes: Synthesis of observations from the coupled boundary layer air–sea transfer experiment. *Bull. Amer. Meteor. Soc.*, **88**, 357–374, https://doi.org/10.1175/BAMS-88-3-357.

Bourassa, M. A., 2000: Shear stress model for the aqueous boundary layer near the air-sea interface. *J. Geophys. Res.*, **105**, 1167–1176, https://doi.org/10.1029/1999JC900250.

——, 2006: Satellite-based observations of surface turbulent stress during severe weather. *WIT Trans. State-Art Sci. Eng.*, **23**, 35–52, https://doi.org/10.2495/978-1-85312-929-2/02.

——, D. G. Vincent, and W. L. Wood, 1999: A flux parameterization including the effects of capillary waves and sea state. *J. Atmos. Sci.*, **56**, 1123–1139, https://doi.org/10.1175/1520-0469(1999)056<1123:AFPITE>2.0.CO;2.

——, and Coauthors, 2019: Remotely sensed winds and wind stresses for marine forecasting and ocean modeling. *Front. Mar. Sci.*, **6**, 443, https://doi.org/10.3389/fmars.2019.00443.

Buck, A. L., 1981: New equations for computing vapor pressure and enhancement factor. *J. Appl. Meteor.*, **20**, 1527–1532, https://doi.org/10.1175/1520-0450(1981)020<1527:NEFCVP>2.0.CO;2.

Businger, J. A., J. C. Wyngaard, Y. Izumi, and E. F. Bradley, 1971: Flux-profile relationships in the atmospheric surface layer. *J. Atmos. Sci.*, **28**, 181–189, https://doi.org/10.1175/1520-0469(1971)028<0181:FPRITA>2.0.CO;2.

Chou, S.-H., 1993: A comparison of airborne eddy correlation and bulk aerodynamic methods for ocean-air turbulent fluxes during cold-air outbreaks. *Bound.-Layer Meteor.*, **64**, 75–100, https://doi.org/10.1007/BF00705663.

Covey, W., 1983: A method for the computation of logarithmic wind profile parameters and their standard errors. *US Dept. Agric. Prod. Res. Rep.*, **72**, 28–33.

Emanuel, K. A., 1986: An air-sea interaction theory for tropical cyclones. Part I: Steady-state maintenance. *J. Atmos. Sci.*, **43**, 585–605, https://doi.org/10.1175/1520-0469(1986)043<0585:AASITF>2.0.CO;2.

——, 1988: The maximum intensity of hurricanes. *J. Atmos. Sci.*, **45**, 1143–1155, https://doi.org/10.1175/1520-0469(1988)045<1143:TMIOH>2.0.CO;2.

——, 1995: Sensitivity of tropical cyclones to surface exchange coefficients and a revised steady-state model incorporating eye dynamics. *J. Atmos. Sci.*, **52**, 3969–3976, https://doi.org/10.1175/1520-0469(1995)052<3969:SOTCTS>2.0.CO;2.

——, 2018: 100 years of progress in tropical cyclone research. *A Century of Progress in Atmospheric and Related Sciences: Celebrating the American Meteorological Society Centennial*, *Meteor. Monogr.*, No. 59, Amer. Meteor. Soc., https://doi.org/10.1175/AMSMONOGRAPHS-D-18-0016.1.

Fairall, C. W., J. D. Kepert, and G. J. Holland, 1994: The effect of sea spray on surface energy transports over the ocean. *Global Atmos. Ocean Syst.*, **2**, 121–142.

——, E. F. Bradley, J. E. Hare, A. A. Grachev, and J. B. Edson, 2003: Bulk parameterization of air–sea fluxes: Updates and verification for the COARE algorithm. *J. Climate*, **16**, 571–591, https://doi.org/10.1175/1520-0442(2003)016<0571:BPOASF>2.0.CO;2.

Feistel, R., D. G. Wright, H.-J. Kretzschmar, E. Hagen, S. Herrmann, and R. Span, 2010: Thermodynamic properties of sea air. *Ocean Sci.*, **6**, 91–141, https://doi.org/10.5194/os-6-91-2010.

Foken, T., 2006: 50 years of the Monin–Obukhov similarity theory. *Bound.-Layer Meteor.*, **119**, 431–447, https://doi.org/10.1007/s10546-006-9048-6.

Franklin, J. L., M. L. Black, and K. Valde, 2003: GPS dropwindsonde wind profiles in hurricanes and their operational implications. *Wea. Forecasting*, **18**, 32–44, https://doi.org/10.1175/1520-0434(2003)018<0032:GDWPIH>2.0.CO;2.

Grachev, A. A., C. W. Fairall, and E. F. Bradley, 2000: Convective profile constants revisited. *Bound.-Layer Meteor.*, **94**, 495–515, https://doi.org/10.1023/A:1002452529672.

Harper, B. A., J. D. Kepert, and J. D. Ginger, 2010: The mean wind. Guidelines for Converting Between Various Wind

Averaging Periods in Tropical Cyclone Conditions, WMO/TD1555, 7–11, https://library.wmo.int/idurl/4/48652.

Hock, T. F., and J. L. Franklin, 1999: The NCAR GPS dropwindsonde. *Bull. Amer. Meteor. Soc.*, **80**, 407–420, https://doi.org/10.1175/1520-0477(1999)080<0407:TNGD>2.0.CO;2.

Holthuijsen, L. H., M. D. Powell, and J. D. Pietrzak, 2012: Wind and waves in extreme hurricanes. *J. Geophys. Res.*, **117**, C09003, https://doi.org/10.1029/2012JC007983.

Howden, S., D. Gilhousen, N. Guinasso, J. Walpert, M. Sturgeon, and L. Bender, 2008: Hurricane Katrina winds measured by a buoy-mounted sonic anemometer. *J. Atmos. Oceanic Technol.*, **25**, 607–616, https://doi.org/10.1175/2007JTECHO518.1.

Kaimal, J. C., J. C. Wyngaard, D. A. Haugen, O. R. Coté, Y. Izumi, S. J. Caughey, and C. J. Readings, 1976: Turbulence structure in the convective boundary layer. *J. Atmos. Sci.*, **33**, 2152–2169, https://doi.org/10.1175/1520-0469(1976)033<2152:TSITCB>2.0.CO;2.

Klotz, B. W., and E. W. Uhlhorn, 2014: Improved stepped frequency microwave radiometer tropical cyclone surface winds in heavy precipitation. *J. Atmos. Oceanic Technol.*, **31**, 2392–2408, https://doi.org/10.1175/JTECH-D-14-00028.1.

Knapp, K. R., M. C. Kruk, D. H. Levinson, H. J. Diamond, and C. J. Neumann, 2010: The International Best Track Archive for Climate Stewardship (IBTrACS): Unifying tropical cyclone data. *Bull. Amer. Meteor. Soc.*, **91**, 363–376, https://doi.org/10.1175/2009BAMS2755.1.

Large, W. G., and S. Pond, 1981: Open ocean momentum flux measurements in moderate to strong winds. *J. Phys. Oceanogr.*, **11**, 324–336, https://doi.org/10.1175/1520-0485(1981)011<0324:OOMFMI>2.0.CO;2.

Liu, W. T., K. B. Katsaros, and J. A. Businger, 1979: Bulk parameterization of air-sea exchanges of heat and water vapor including the molecular constraints at the interface. *J. Atmos. Sci.*, **36**, 1722–1735, https://doi.org/10.1175/1520-0469(1979)036<1722:BPOASE>2.0.CO;2.

Martin, C., and I. Suhr, 2021: NCAR/EOL Atmospheric Sounding Processing Environment (ASPEN) software, version 3.4.5. NCAR, https://www.eol.ucar.edu/content/aspen.

Monin, A. S., and A. M. Obukhov, 1954: Basic laws of turbulent mixing in the surface layer of the atmosphere. *Tr. Akad. Nauk SSSR Geophiz. Inst.*, **24**, 163–187.

NOAA-NHC, 2021: Saffir-Simpson Hurricane Wind Scale. National Hurricane Center, accessed 31 March 2022, https://www.nhc.noaa.gov/aboutsshws.php.

Obukhov, A. M., 1946: "Turbulentnost" v temperaturnoj-neodnorodnoj atmosfere. *Tr. Inst. Theor. Geofiz. Akad. Nauk SSSR*, **1**, 95–115.

——, 1971: Turbulence in an atmosphere with a non-uniform temperature. *Bound.-Layer Meteor.*, **2**, 7–29, https://doi.org/10.1007/BF00718085.

PopStefanija, I., C. W. Fairall, and E. J. Walsh, 2021: Mapping of directional ocean wave spectra in hurricanes and other environments. *IEEE Trans. Geosci. Remote Sens.*, **59**, 9007–9020, https://doi.org/10.1109/TGRS.2020.3042904.

Powell, M. D., 2006: Drag coefficient distribution and wind speed dependence in tropical cyclones. Joint Hurricane Testbed Program Final Rep., 26 pp.

——, P. J. Vickery, and T. A. Reinhold, 2003: Reduced drag coefficient for high wind speeds in tropical cyclones. *Nature*, **422**, 279–283, https://doi.org/10.1038/nature01481.

Powell, M. J. D., 1964: An efficient method for finding the minimum of a function of several variables without calculating derivatives. *Comput. J.*, **7**, 155–162, https://doi.org/10.1093/comjnl/7.2.155.

Prandtl, L., 1925: 7. Bericht über untersuchungen zur ausgebildeten turbulenz. *Z. Angew. Math. Mech.*, **5**, 136–139, https://doi.org/10.1002/zamm.19250050212.

Richter, D. H., C. Wainwright, D. P. Stern, G. H. Bryan, and D. Chavas, 2021: Potential low bias in high-wind drag coefficient inferred from dropsonde data in hurricanes. *J. Atmos. Sci.*, **78**, 2339–2352, https://doi.org/10.1175/JAS-D-20-0390.1.

Saffir, H. S., 1973: Hurricane wind and storm surge. *Mil. Eng.*, **423**, 4–5.

Schott, T., and Coauthors, 2019: The Saffir-Simpson Hurricane Wind Scale. 4 pp., https://www.nhc.noaa.gov/pdf/sshws.pdf.

Shen, W., and I. Ginis, 2003: Effects of surface heat flux-induced sea surface temperature changes on tropical cyclone intensity. *Geophys. Res. Lett.*, **30**, 1933, https://doi.org/10.1029/2003GL017878.

Simpson, R. H., 1974: The hurricane disaster—Potential scale. *Weatherwise*, **27**, 169–186, https://doi.org/10.1080/00431672.1974.9931702.

Smith, S. D., 1988: Coefficients for sea surface wind stress, heat flux, and wind profiles as a function of wind speed and temperature. *J. Geophys. Res.*, **93**, 15 467–15 472, https://doi.org/10.1029/JC093iC12p15467.

Stopa, J. E., C. Wang, D. Vandemark, R. Foster, A. Mouche, and B. Chapron, 2022: Automated global classification of surface layer stratification using high-resolution sea surface roughness measurements by satellite synthetic aperture radar. *Geophys. Res. Lett.*, **49**, e2022GL098686, https://doi.org/10.1029/2022GL098686.

Stull, R. B., 1988a: Mixing length theory. *An Introduction to Boundary Layer Meteorology*, Kluwer Academic Publishers, 206–208.

——, 1988b: The log wind profile. *An Introduction to Boundary Layer Meteorology*, Kluwer Academic Publishers, 376–386.

Troitskaya, Y., D. Sergeev, A. Kandaurov, M. Vdovin, and S. Zilitinkevich, 2019: The effect of foam on waves and the aerodynamic roughness of the water surface at high winds. *J. Phys. Oceanogr.*, **49**, 959–981, https://doi.org/10.1175/JPO-D-18-0168.1.

UCAR/NCAR–Earth Observing Laboratory, 1993: NCAR Airborne Vertical Atmospheric Profiling System (AVAPS). Accessed 31 March 2022, https://doi.org/10.5065/D66W9848.

Uhlhorn, E. W., and P. G. Black, 2003: Verification of remotely sensed sea surface winds in hurricanes. *J. Atmos. Oceanic Technol.*, **20**, 99–116, https://doi.org/10.1175/1520-0426(2003)020<0099:VORSSS>2.0.CO;2.

——, ——, J. L. Franklin, M. Goodberlet, J. Carswell, and A. S. Goldstein, 2007: Hurricane surface wind measurements from an operational stepped frequency microwave radiometer. *Mon. Wea. Rev.*, **135**, 3070–3085, https://doi.org/10.1175/MWR3454.1.

Virtanen, P., and Coauthors, 2020: SciPy 1.0: Fundamental algorithms for scientific computing in Python. *Nat. Methods*, **17**, 261–272, https://doi.org/10.1038/s41592-019-0686-2.

Walsh, E. J., C. W. Fairall, and I. PopStefanija, 2021: In the eye of the storm. *J. Phys. Oceanogr.*, **51**, 1835–1842, https://doi.org/10.1175/JPO-D-20-0219.1.

Wang, J., and Coauthors, 2015: A long-term, high-quality, high-vertical-resolution GPS dropsonde dataset for hurricane and other studies. *Bull. Amer. Meteor. Soc.*, **96**, 961–973, https://doi.org/10.1175/BAMS-D-13-00203.1.

Wright, C. W., and Coauthors, 2001: Hurricane directional wave spectrum spatial variation in the open ocean. *J. Phys. Oceanogr.*, **31**, 2472–2488, https://doi.org/10.1175/1520-0485(2001)031<2472:HDWSSV>2.0.CO;2.

Wright, E. E., M. A. Bourassa, A. Stoffelen, and J.-R. Bidlot, 2021: Characterizing buoy wind speed error in high winds and varying sea state with ASCAT and ERA5. *Remote Sens.*, **13**, 4558, https://doi.org/10.3390/rs13224558.

Yang, S., D. W. Shin, S. Cocke, C. C. Nam, M. Bourassa, D.-H. Cha, and B.-M. Kim, 2024: Unveiling the pivotal influence of sea spray heat fluxes on hurricane rapid intensification. *Environ. Res. Lett.*, **19**, 114058, https://doi.org/10.1088/1748-9326/ad7ee0.

——, and Coauthors, 2025: Sea spray effects on typhoon prediction in the Yellow and East China Seas: Case studies using a coupled atmosphere-ocean-wave model for Lingling (2019) and Maysak (2020). *Environ. Res. Lett.*, **20**, 054028, https://doi.org/10.1088/1748-9326/adc616.